RESEARCH ARTICLE

Near-Field Reception of Dipole Sources Using a Dual-Loaded Loop

CHRISTOPHER G. HYNES®, (Student Member, IEEE), AND
RODNEY G. VAUGHAN®, (Life Fellow, IEEE)
School of Engineering Science, Simon Fraser University, Burnaby, BC V5A 1S6, Canada
Corresponding author: Christopher G. Hynes (c_h@sfu.ca)

ABSTRACT The dual-loaded loop is a two-port antenna configured as two half-loops. Its advantage is the ability to sense two field components instead of the single component of a single-port loop. In this study, the theory of the dual-loaded loop is extended to cases for sensing arbitrarily located electric and magnetic dipole sources. New general expressions are presented for the tangential electric field on a loop resulting from electric and magnetic dipole sources. From these field expressions, closed-form approximations for the currents at the ports are obtained. The approximations are shown to be very accurate through simulation, but can degrade when the separation distance between the dipole source and loop is small. The worst discrepancy occurs when an electric dipole is close to and aligned with one of the ports. These expressions provide a benchmark for checking numerical and physical results for this class of sensor.

INDEX TERMS Dipole antennas, electromagnetic fields, electrically small antennas, Fourier series, loop antennas, near fields, probe antennas.

I. INTRODUCTION

The dual-loaded loop is an established antenna that is primarily used as an electrically small electromagnetic field sensor. A straightforward beamformer (combining the port signals) allows the simultaneous measurement of a component of both the electric and magnetic fields. When three dual-loaded loop sensors are co-located but oriented orthogonally, the system can detect all six components of an electromagnetic field. Such systems have been used in Electromagnetic Compatibility (EMC) testing for low-frequency emissions [1] and direction-finding [2], [3], [4], [5], [6], [7], but could also be useful in novel applications such as earthquake pre-detection [8] and biomedical engineering [9].

The analysis of the dual-loaded loop is based on loop antenna theory. The loop antenna is a fundamental element that has been well analyzed [10]. Some of the breakthroughs particularly relevant to the dual-loaded loop are as follows. Pocklington's seminal work in 1897 [11] considered an arbitrary current distribution on a circular loop by expressing it in terms of a Fourier series. Hallén [12] expressed the current and impedance of a loaded electrically thin loop, however, the formulation contained a singularity that made

the series quasi-convergent and applicable only to electrically small loops. The convergence issues were addressed around 1960 by Storer [13] and Wu [14], allowing the analysis of electrically larger loops. The Fourier techniques of these landmark works have provided a general framework for analyzing loop currents from general incident fields, allowing single-port loops to be extended to multiple-port loops [15], [16]. In addition to the Fourier techniques of analyzing loop antennas, some works have considered a more circuit-based approach [7], [17], and others have used different basis-function expansion methods [18], [19], [20]. Whiteside and King [15] showed that an electrically small, dual-loaded loop can simultaneously detect both the electric and magnetic intensities from incident plane waves. Around the 1980s, Kanda [21] extended Whiteside and King's analysis to general incident field distributions, and Kanda and Hill [22] showed that a dual-loaded loop can be used to detect a field component from electric and magnetic dipole sources that are located at the center of the loop. There have been recent contributions to the theory of multi-loaded loops, for example, [7], [17], [23].

Closed-form expressions enable practical and rapid calculations for complex situations within an otherwise complex formulation. They have been established for the responses of the dual-loaded loop to incident plane waves [21], [24], and

centrally located electric and magnetic dipole sources [22]. However, there is scant treatment for the spatial dependence of dipole sources, which is of practical importance. Specifically, Novotny et al. [25] investigated positional sensitivity by measuring an offset spherical dipole radiator. They considered only the total combined output power from the loop ports and found that if the electric dipole source was within a sphere of 72% of the loop radius then the power was within 3 ± 1.5 dB of the center value. This initial investigation was primarily concerned with centrally located sources and only incidentally considered the spatial dependence of the coupling from dipole sources to dual-loaded loops. Tofani et al. [26] measured the field responses from dipole sources along the Cartesian axes using field meters. They then compared the field values to those calculated from dipoles that were measured at the center of a three-loop antenna system. Although this study investigated the fields away from dipole sources, it did not examine the spatial dependence of the coupling from offset dipole sources to a three-loop antenna system or a dual-loaded loop. To the best of our knowledge, no other studies have been undertaken to investigate the spatial dependence of the coupling from dipole sources to a dual-loaded loop.

This paper extends the theory of dual-loaded loop sensors to off-center electric or magnetic dipole sources. Some examples of closed-form expressions being particularly useful are as follows. Dual-loaded loops are commonly deployed near ground planes, and the new contributions allow ground plane effects to be predicted using image theory for the source. The pathloss between the dipole source and loop ports becomes available as a function of the spherical position and allows for calculating practical performance metrics such as potential noise power, i.e., how far potential noise sources must be kept from the loop. The extensions also enable better source-type discrimination, i.e., the quantification of electric and magnetic dipoles, by providing discrimination as a function of position. Finally, the formulations offer a way to avert time-consuming simulations or experiments for the off-center cases and provide an analytical reference against which such results, or numerical integral calculations, can be compared.

The accuracy of approximating the loop current in terms of only the low-ordered Fourier coefficients is included in this work. Although the expressions for the Fourier coefficients are accurate, inaccuracies can arise when approximating the loop currents for a specific configuration – when the electric dipole source is aligned with and near the loop. The approximation for the loop current from a magnetic dipole is shown to be accurate across all off-center positions investigated.

A motivation for this work is to use a three-loop antenna system [22], comprising three electrically small orthogonal dual-loaded loops. As noted above, the three-loop antenna system, with a 6-port beamformer, allows the simultaneous detection of the six electromagnetic field components. An application is to research potential biological emissions, such as those from the brain in electroencephalography. Such
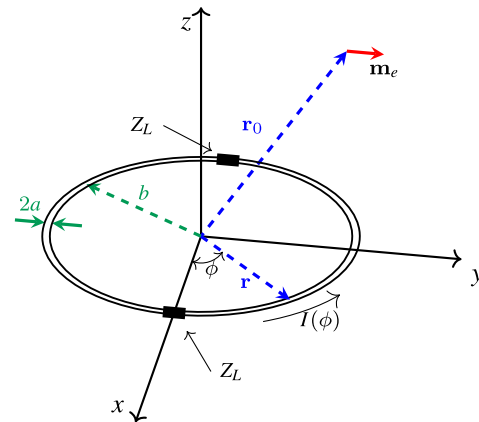
FIGURE 1. Dual-loaded wire loop with an off-center dipole source. The loop is centered in the *xy*-plane with port at $x = \pm b$. The radius of the loop is *b* meters, and the radius of the wire is *a* meters.

emissions are likely at extremely low frequencies, and thus even physically large loops are electrically extremely small. Although this example is for low frequencies, typically less than 40 Hz, electrically compact antennas are always of great interest at any frequency (although they have known limitations on bandwidth) and the formulation herein is for any frequency. In analyzing the performance of such a device, the starting point is the general treatment of the coupling between a single dual-loaded loop and off-center sources.

The remainder of this paper is organized as follows. Section II presents the background theory of a dual-loaded loop sensor. Section III extends this theory by deriving the general Fourier series coefficients for the tangential electric field along a dual-loaded loop from offset electric and magnetic dipole sources. From these general Fourier coefficients, closed-form expressions are determined for the dipole- and loop-mode Fourier coefficients, as well as simplified first-order approximations that are accurate when the separation distance is small. Finally, Section IV investigates the accuracy of the theory against the simulation results. Lengthy expressions are confined to the Appendices, with concise directions for their derivation.

II. BACKGROUND
Throughout this paper, the electromagnetic fields are assumed time-harmonic and the time-harmonic term $e^{-j\omega t}$ is suppressed.

A. DUAL-LOADED LOOP PORT CURRENTS
This section briefly summarizes the background formulation of the current on a dual-loaded loop induced from a general incident electromagnetic field that was presented in [21]. Unless stated otherwise, all the formulas within this section were produced in [21] and will be used in the following sections.

The dual-loaded loop, as shown in Fig. 1, is centered in the *xy*-plane and is electrically small and thin, such that

$a \ll b, ka \ll 1$, where b is the loop radius, a is the wire radius, and k is the wavenumber. The boundary condition on a perfectly conducting loop, with two loads diametrically opposite at $(x, y, z) = (\pm b, 0, 0)$, is that the tangential electric field is zero everywhere except across the infinitesimal gap supporting the loads, i.e.,

$$-I(\phi = 0)Z_L\delta(\phi) - I(\phi = \pi)Z_L\delta(\phi - \pi)$$
$$= bE_\phi^i(b, \phi) + \frac{j\eta}{4\pi}\int_{-\pi}^{\pi} L(\phi - \phi')I(\phi')d\phi', \tag{1}$$

where η is the wave impedance in the medium and Z_L is the port impedance. The tangential component of the incident electric field on the loop surface, $E_\phi^i(b, \phi)$, the integral kernel, $L(\phi - \phi')$, and the loop current, $I(\phi)$, can all be expressed as Fourier series:

$$E_\phi^i(b, \phi) = \sum_{-\infty}^{\infty} f_n e^{-jn\phi} \Rightarrow f_n = \frac{1}{2\pi}\int_{-\pi}^{\pi} E_\phi^i(b, \phi)e^{jn\phi}d\phi, \tag{2}$$

$$I(\phi) = \sum_{-\infty}^{\infty} I_n e^{-jn\phi} \Rightarrow I_n = \frac{1}{2\pi}\int_{-\pi}^{\pi} I(\phi)e^{jn\phi}d\phi, \tag{3}$$

$$L(\phi) = \sum_{-\infty}^{\infty} a_n e^{-jn\phi}, \tag{4}$$

$$a_n = a_{-n} = \frac{kb}{2}(N_{n+1} + N_{n-1}) - \frac{n^2}{kb}N_n, \tag{5}$$

$$N_n = N_{-n} = \frac{1}{\pi}K_0\left(\frac{na}{b}\right)\dot{I}_0\left(\frac{na}{b}\right)$$
$$- \frac{1}{2}\int_0^{2kb}(\Omega_{2n}(x) + jJ_{2n}(x))\,dx \tag{6}$$
$$+ \frac{1}{\pi}\left(\ln 4n + \gamma - 2\sum_{m=0}^{n-1}\frac{1}{2m+1}\right), \quad n \neq 0$$

$$N_0 = \frac{1}{\pi}\ln\frac{8b}{a} - \frac{1}{2}\int_0^{2kb}(\Omega_0(x) + jJ_0(x))\,dx, \tag{7}$$

where Ω_n is the Lommel-Weber function, J_n is the Bessel function, $\gamma = 0.5772\cdots$ is Euler's constant, and $\dot{I}_0$ and K_0 are the modified Bessel functions of the first and second kind, respectively.

Substituting (2), (3) and (4) into (1) and integrating yields the Fourier series

$$-I(0)Z_L\delta(\phi) - I(\pi)Z_L\delta(\phi - \pi) = \sum_{-\infty}^{\infty}\left(\frac{j\eta}{2}a_n I_n + bf_n\right)e^{-jn\phi}. \tag{8}$$

with Fourier series coefficients

$$\frac{j\eta}{2}a_n I_n + bf_n$$
$$= \frac{1}{2\pi}\int_{-\pi}^{\pi}(-I(0)Z_L\delta(\phi) - I(\pi)Z_L\delta(\phi - \pi))\,e^{jn\phi}d\phi, \tag{9}$$
$$= -\frac{Z_L}{2\pi}\left(I(0) + I(\pi)e^{jn\pi}\right). \tag{10}$$

Solving for the Fourier series coefficients for the loop current yields

$$I_n = \frac{j}{\pi\eta a_n}\left(2\pi bf_n + Z_L\left(I(0) + I(\pi)e^{jn\pi}\right)\right). \tag{11}$$

For electrically small loops, the current can be approximated from the first few coefficients ($|n| \leq 1$) of its Fourier series. When this is done, using (3) and (11), the difference in current between the two ports is

$$I_\Delta = \frac{1}{2}(I(0) - I(\pi))$$
$$= \sum_{n\text{ odd}} I_n = -\frac{2\pi b}{j\pi\eta + 2Z_L\sum_{n\text{ odd}}\frac{1}{a_n}}\sum_{n\text{ odd}}\frac{f_n}{a_n} \tag{12}$$
$$\approx I_1 + I_{-1} = -\frac{\pi bY_1}{1 + 2Z_L Y_1}(f_1 + f_{-1}), \tag{13}$$

where $Y_1 = 2/j\eta\pi a_1$ is the admittance of the $n = 1$ current mode.

The sum of the two port currents is

$$I_\Sigma = \frac{1}{2}(I(0) + I(\pi))$$
$$= \sum_{n\text{ even}} I_n = -\frac{2\pi b}{j\pi\eta + 2Z_L\sum_{n\text{ even}}\frac{1}{a_n}}\sum_{n\text{ even}}\frac{f_n}{a_n} \tag{14}$$
$$\approx I_0 = -\frac{2\pi bY_0}{1 + 2Z_L Y_0}f_0, \tag{15}$$

where $Y_0 = 1/j\eta\pi a_0$ is the admittance of the $n = 0$ current mode.

In what follows, the Fourier coefficient term $f_1 + f_{-1}$ will be referred to as the dipole-mode, and the term f_0 as the loop-mode.

B. LOOP RESPONSE TO CENTRALLY LOCATED DIPOLE SOURCES

Kanda and Hill [22] considered the case of electric and magnetic dipole moments at the center of a loop:

$$\mathbf{m}_e = \lim_{V\to 0}\int_V \mathbf{J}dV = m_{e,x}\mathbf{u}_x + m_{e,y}\mathbf{u}_y + m_{e,z}\mathbf{u}_z, \tag{16}$$

$$\mathbf{m}_m = \lim_{V\to 0}\int_V \mathbf{r} \times \mathbf{J}dV = m_{m,x}\mathbf{u}_x + m_{m,y}\mathbf{u}_y + m_{m,z}\mathbf{u}_z, \tag{17}$$

where $\mathbf{u}_i$ is the ith Cartesian unit vector, $m_{e,i}$ and $m_{m,i}$ are the components of the electric and magnetic dipole moments

along the ith Cartesian coordinate, respectively, $\mathbf{J}$ is the electric current density, and V is the electrically small volume in which the electric current density is located. The ϕ-component of the electric field is tangential to the loop and is given by [22]

$$E_\phi^i(b, \phi) = m_{m,z}G_m + m_{e,y}G_e \cos \phi - m_{e,x}G_e \sin \phi, \quad (18)$$

where

$$G_m = \frac{\eta}{4\pi} \left(\frac{k^2}{b} + \frac{jk}{b^2} \right) e^{jkb}, \quad (19)$$

$$G_e = \frac{\eta}{4\pi} \left(\frac{jk}{b} - \frac{1}{b^2} + \frac{1}{jkb^3} \right) e^{jkb}. \quad (20)$$

From (2), the Fourier series coefficients for (18) are [27]

$$f_0 = m_{m,z}G_m, \quad (21)$$

$$f_1 = \frac{m_{e,y}G_e}{2} + \frac{m_{e,x}G_e}{2j}, \quad (22)$$

$$f_{-1} = \frac{m_{e,y}G_e}{2} - \frac{m_{e,x}G_e}{2j}. \quad (23)$$

Using the Fourier coefficients (22)-(23) in (13), and (21) in (15), relates the summation and difference currents to the components of the electric and magnetic moments at the center of the dual-loaded loop [27],

$$I_\Delta \approx -\frac{\pi b Y_1 G_e}{1 + 2Y_1 Z_L} m_{e,y}, \quad (24)$$

$$I_\Sigma \approx -\frac{2\pi b Y_0 G_m}{1 + 2Y_0 Z_L} m_{m,z}. \quad (25)$$

Note that (24) is half of the value presented in previous studies [22], [25], [26].

III. THEORY
A. ELECTRIC DIPOLE SOURCE
The electric field at spherical coordinate $\mathbf{r}$ from an electric dipole $\mathbf{m}_e$ located at $\mathbf{r}_0 = x_0\mathbf{u}_x + y_0\mathbf{u}_y + z_0\mathbf{u}_z$ is [28]

$$\mathbf{E}_e(\mathbf{r}) = \frac{j\eta e^{jk|\mathbf{r}-\mathbf{r}_0|}}{4\pi k} \left[\frac{k^2}{|\mathbf{r}-\mathbf{r}_0|^3} (\mathbf{r}-\mathbf{r}_0) \times (\mathbf{m}_e \times (\mathbf{r}-\mathbf{r}_0)) \right.$$
$$+ \left(\frac{3(\mathbf{r}-\mathbf{r}_0)((\mathbf{r}-\mathbf{r}_0) \cdot \mathbf{m}_e)}{|\mathbf{r}-\mathbf{r}_0|^2} - \mathbf{m}_e \right) \times$$
$$\left. \left(\frac{1}{|\mathbf{r}-\mathbf{r}_0|^3} - \frac{jk}{|\mathbf{r}-\mathbf{r}_0|^2} \right) \right]. \quad (26)$$

The ϕ-component of the electric field along a loop is

$$E_{e,\phi} = -\sin \phi E_{e,x} + \cos \phi E_{e,y}, \quad (27)$$

$$= \frac{j\eta}{4\pi} k^4 e^{j\sqrt{\hat{R}^2 - 2k^2 b(x_0 \cos \phi + y_0 \sin \phi)}} \times$$
$$\left(\frac{B' \sin \phi + C' \cos \phi + D \sin 2\phi + E \cos 2\phi - 3F/5}{(\hat{R}^2 - 2k^2 b(x_0 \cos \phi + y_0 \sin \phi))^{3/2}} \right.$$
$$+ \frac{B \sin \phi + C \cos \phi + D \sin 2\phi + E \cos 2\phi + F}{(\hat{R}^2 - 2k^2 b(x_0 \cos \phi + y_0 \sin \phi))^{5/2}}$$
$$\left. -j \frac{B \sin \phi + C \cos \phi + D \sin 2\phi + E \cos 2\phi + F}{(\hat{R}^2 - 2k^2 b(x_0 \cos \phi + y_0 \sin \phi))^2} \right), \quad (28)$$

where

$$|\mathbf{r} - \mathbf{r}_0| = \sqrt{R^2 - 2b(x_0 \cos \phi + y_0 \sin \phi)}, \quad (29)$$

$$R^2 = b^2 + r_0^2, \quad (30)$$

$$\hat{R} = kR, \quad (31)$$

$$B' = x_0 \mathbf{m}_e \cdot \mathbf{r}_0 - R^2 m_{e,x}, \quad (32)$$

$$C' = -y_0 \mathbf{m}_e \cdot \mathbf{r}_0 + R^2 m_{e,y}, \quad (33)$$

$$B = R^2 m_{e,x} - 3x_0 \mathbf{m}_e \cdot \mathbf{r}_0, \quad (34)$$

$$C = -R^2 m_{e,y} + 3y_0 \mathbf{m}_e \cdot \mathbf{r}_0, \quad (35)$$

$$D = \frac{b}{2}(x_0 m_{e,x} - y_0 m_{e,y}), \quad (36)$$

$$E = -\frac{b}{2}(x_0 m_{e,y} + y_0 m_{e,x}), \quad (37)$$

$$F = \frac{5}{2}b(x_0 m_{e,y} - y_0 m_{e,x}). \quad (38)$$

From (2), the Fourier coefficients of (28) are

$$f_n^{(e)} = \frac{j\eta k^4}{8\pi^2} \times$$
$$\int_0^{2\pi} \left(\frac{B' \sin \phi + C' \cos \phi + D \sin 2\phi + E \cos 2\phi - \frac{3F}{5}}{(\hat{R}^2 - 2k^2 b(x_0 \cos \phi + y_0 \sin \phi))^{3/2}} \right.$$
$$+ \frac{B \sin \phi + C \cos \phi + D \sin 2\phi + E \cos 2\phi + F}{(\hat{R}^2 - 2k^2 b(x_0 \cos \phi + y_0 \sin \phi))^{5/2}}$$
$$\left. -j \frac{B \sin \phi + C \cos \phi + D \sin 2\phi + E \cos 2\phi + F}{(\hat{R}^2 - 2k^2 b(x_0 \cos \phi + y_0 \sin \phi))^2} \right)$$
$$e^{j\sqrt{\hat{R}^2 - 2k^2 b(x_0 \cos \phi + y_0 \sin \phi)}} e^{jn\phi} d\phi. \quad (39)$$

(39) can be used to calculate the Fourier coefficients for any n, thereby determining the loop current for any electric dipole position and orientation.

It is useful to have closed-formed expressions for this integral. In the Appendix, (39) is expressed as the closed-form approximation (83). To offer a sense of the dominance of the leading term of the expression, for a small distance R, i.e., $kR < 0.5$, (83) is within 1 dB of its leading order term of kR, expressed as

$$f_1^{(e)} + f_{-1}^{(e)} \approx \frac{j\eta b^2 e^{jkR}}{4\pi k R^7} \left[(c - \epsilon) \, _2F_1 \left(\frac{5}{4}, \frac{7}{4}; 1; \zeta \right) \right.$$
$$+ \frac{5}{4}(5d + \zeta\epsilon) \, _2F_1 \left(\frac{7}{4}, \frac{9}{4}; 2; \zeta \right)$$
$$- \frac{35}{32}(4d + \zeta c) \, _2F_1 \left(\frac{9}{4}, \frac{11}{4}; 3; \zeta \right)$$
$$\left. - \frac{105}{128} \zeta d \, _2F_1 \left(\frac{11}{4}, \frac{13}{4}; 4; \zeta \right) \right], \quad (40)$$

where

$$\zeta = \frac{4b^2(x_0^2 + y_0^2)}{R^4}, \quad (41)$$

$$c = \frac{3R^2 y_0}{b^2} \mathbf{m}_e \cdot \mathbf{r}_0, \quad (42)$$

$$d = (x_0^2 - y_0^2)m_{e,y} - 2x_0 y_0 m_{e,x}, \quad (43)$$

$$\epsilon = \frac{R^4}{b^2} m_{e,y}, \tag{44}$$

and $_2F_1(\cdot, \cdot; \cdot; \cdot)$ is the Gaussian hypergeometric function. In the limit of small kb, (40) agrees with $f_{-1}^{(e)} + f_1^{(e)}$ obtained from (22) and (23) at the center of the loop, i.e., $r_0 = 0$.

Although the dipole-mode is the dominant mode for an electric dipole source located near the center of a dual-loaded loop, it is of particular interest to determine the positional dependence of the loop-mode that is generated. The full expression for $f_0^{(e)}$ is given by (84). For small $\hat{R}$, i.e., $\hat{R} = kR < 0.5$, the $\hat{R}$ terms can be ignored, resulting in an expression within 1 dB of (84)

$$f_0^{(e)} \approx \frac{jkb\eta e^{jkR}}{2\pi R^3} \frac{(\mathbf{m}_e \times \mathbf{r}_0)_z}{\zeta} \times$$
$$\left[(\zeta - 5) \, _2F_1 \left(\frac{3}{4}, \frac{5}{4}; 1; \zeta \right) \right.$$
$$\left. - 5(\zeta - 1) \, _2F_1 \left(\frac{3}{4}, \frac{9}{4}; 1; \zeta \right) \right]. \tag{45}$$

B. MAGNETIC DIPOLE SOURCE

The electric field at spherical coordinate $\mathbf{r}$ from a magnetic dipole $\mathbf{m}_m$ located at $\mathbf{r}_0 = x_0 \mathbf{u}_x + y_0 \mathbf{u}_y + z_0 \mathbf{u}_z$ is [29]

$$\mathbf{E}_m(\mathbf{r}) = \frac{k^2 \eta e^{jk|\mathbf{r}-\mathbf{r}_0|}}{4\pi} \times$$
$$\left(\frac{1}{|\mathbf{r} - \mathbf{r}_0|^2} + \frac{j}{k|\mathbf{r} - \mathbf{r}_0|^3} \right) \mathbf{m}_m \times (\mathbf{r} - \mathbf{r}_0). \tag{46}$$

The ϕ-component of the electric field is

$$E_{m,\phi} = -\sin\phi E_{m,x} + \cos\phi E_{m,y}, \tag{47}$$
$$= \frac{k^4 \eta}{4\pi} e^{j\sqrt{\hat{R}^2 - 2k^2 b(x_0 \cos\phi + y_0 \sin\phi)}} \times$$
$$\left[bm_{m,z} + G\sin\phi + H\cos\phi \right] \times$$
$$\left(\frac{1}{\hat{R}^2 - 2k^2 b(x_0 \cos\phi + y_0 \sin\phi)} + \right.$$
$$\left. + j \frac{1}{(\hat{R}^2 - 2k^2 b(x_0 \cos\phi + y_0 \sin\phi))^{3/2}} \right), \tag{48}$$

where

$$G = m_{m,y} z_0 - m_{m,z} y_0 = (\mathbf{m}_m \times \mathbf{r}_0)_x, \tag{49}$$
$$H = m_{m,x} z_0 - m_{m,z} x_0 = -(\mathbf{m}_m \times \mathbf{r}_0)_y, \tag{50}$$

and $(\cdot)_i$ denotes the i Cartesian component of the vector.

Using (2), the Fourier coefficients of (48) are

$$f_n^{(m)} = \frac{k^4 \eta}{8\pi^2} \int_0^{2\pi} d\phi e^{jn\phi} \left[bm_{m,z} + G\sin\phi + H\cos\phi \right] \times$$
$$\left(\frac{1}{\hat{R}^2 - 2k^2 b(x_0 \cos\phi + y_0 \sin\phi)} + \right.$$
$$\left. + j \frac{1}{(\hat{R}^2 - 2k^2 b(x_0 \cos\phi + y_0 \sin\phi))^{3/2}} \right) \times$$
$$e^{j\sqrt{\hat{R}^2 - 2k^2 b(x_0 \cos\phi + y_0 \sin\phi)}}. \tag{51}$$

(51) can be used to calculate the Fourier coefficients for any n, thereby determining the loop current for any magnetic dipole position and orientation.

As for the electric dipole source above, it is useful to have closed-formed expressions for this integral. In the Appendix, (51) is expressed as the closed-form approximation (85). For small $\hat{R}$, the $\hat{R}$ terms can be ignored, reducing (85) to

$$f_0^{(m)} \approx \frac{jkb\eta e^{jkR}}{4\pi R^3} \left[m_{m,z} \, _2F_1 \left(\frac{3}{4}, \frac{5}{4}; 1; \zeta \right) \right.$$
$$\left. + \frac{3}{2} \frac{((\mathbf{m}_m \times \mathbf{r}_0) \times \mathbf{r}_0)_z}{R^2} \, _2F_1 \left(\frac{5}{4}, \frac{7}{4}; 2; \zeta \right) \right], \tag{52}$$

which is within 1 dB of (85) when $kR < 0.5$. In the limit of small kb, (52) agrees with (21) at the center of the loop, i.e., $r_0 = 0$.

Again, it is of particular interest to determine the positional dependence of the dipole-mode generated from a loop-mode source. From (78), the formula for $f_{-1}^{(m)} + f_1^{(m)}$ can be expressed as (86). For $kR < 0.5$, (86) is within 1 dB of the leading order term of kR,

$$f_1^{(m)} + f_{-1}^{(m)} \approx \frac{jkb^2 \eta e^{jkR}}{4\pi R^5} \left[3x_0 m_{m,z} \, _2F_1 \left(\frac{5}{4}, \frac{7}{4}; 2; \zeta \right) \right.$$
$$- \frac{R^2}{b^2} (\mathbf{m}_m \times \mathbf{r}_0)_y \, _2F_1 \left(\frac{3}{4}, \frac{5}{4}; 1; \zeta \right)$$
$$+ \frac{15}{8R^2} \left((\mathbf{m}_m \times \mathbf{r}_0)_x 2x_0 y_0 \right.$$
$$- (\mathbf{m}_m \times \mathbf{r}_0)_y (x_0^2 - y_0^2) \Big) \times$$
$$\left. _2F_1 \left(\frac{7}{4}, \frac{9}{4}; 3; \zeta \right) \right]. \tag{53}$$

## IV. VERIFICATION AND RESULTS

A. ELECTRIC DIPOLE SOURCE

A small electric dipole with a dual-loaded loop was simulated using CST Microwave Studio's method of moments solver [30]. Fig. 2 shows the simulation model of the electric dipole source. The dual-loaded loop, with an electrical radius of $kb = 0.1$ rad and a wire radius of $ka = 2 \times 10^{-3}$ rad, was centered in the xy-plane with the ports loaded with 315 Ω and located on the x-axis at $\pm b$. The port gaps have an electrical separation of 4×10^{-4} rad. The short y-directed dipole, of electrical length 1.2×10^{-3} rad, was shifted along the Cartesian coordinate axes.

1) VERIFICATION OF THE THEORETICAL PORT CURRENTS FROM AN ELECTRIC DIPOLE

Fig. 3 shows the matching between the theoretical and simulated I_Δ and I_Σ port currents as the electric dipole is shifted along the Cartesian axes. The theoretical I_Δ and I_Σ currents were calculated using Python implementing (12) and (14), respectively, with (5) and (39).

The number of current Fourier series coefficients required to model the port currents accurately depended on the electric dipole proximity to the loop and along which axis the
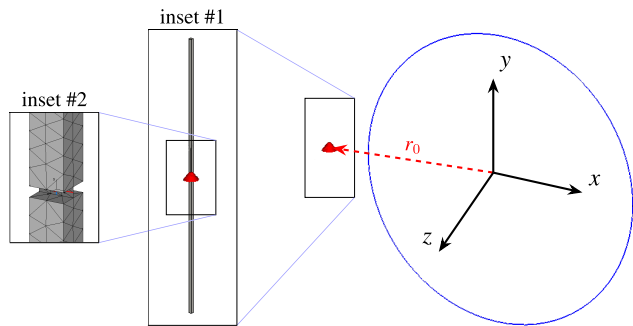
FIGURE 2. The simulation model to determine the Fourier series coefficients of E_ϕ along a circle with an electrical radius of $kb = 0.1$ rad. This example shows a y-directed electric dipole of electrical length 1.2×10^{-3} rad, shifted by the vector r_0, depicted here along the $-x$-direction. Inset #2 shows the meshing used for the method of moments.

dipole was shifted. Fig. 3 shows that achieving accurate port current estimates near the loop requires current Fourier series coefficients up to $n = \pm 17$ for shifts along the x-axis, up to $n = \pm 5$ for shifts along the y-axis, and only the first-order $n = \pm 1$ coefficients for shifts along the z-axis. As shown in Fig. 4, this is due to the loop current having an impulse-like distribution, thereby containing numerous significant Fourier series coefficients when the electric dipole is very close to the loop.

2) EVALUATION OF FIRST-ORDER PORT CURRENT ESTIMATES FROM AN ELECTRIC DIPOLE

As the electric dipole was shifted in the simulation model, the port currents and E_ϕ along the loop were collected. The Fourier series for E_ϕ was used to verify the first-order Fourier coefficients predicted by the new theory.

Fig. 5 compares the first-order Fourier series coefficients of the port current obtained through simulation and theory for an electric dipole source. These plots are normalized to the response when the dipole is at the center of the loop. The expressions (83) for the dipole-mode and (84) for the loop-mode match the Fourier coefficients determined from the E_ϕ field obtained from simulation. The leading term approximations, (40) for the dipole-mode and (45) for the loop-mode, are shown to be very accurate when the dipole off-center distance is electrically small, being within 1 dB when $kR < 0.5$. However, the accuracy degrades as the offset increases.

Fig. 5 also compares the port current approximations using the first-order Fourier series estimates (13) and (15). Good agreement occurs at most dipole offsets, except where the dipole is near the loop. As mentioned above, the worst case occurs when the dipole is aligned with, and approaches, one of the ports. The error is highlighted in Fig. 6, where the various approximations for the port difference current, I_Δ using (13), are compared against the simulated port current, with a worst-case discrepancy of up to 14 dB. This discrepancy stems from the loop current being poorly modelled by the low-order Fourier coefficients for those conditions,
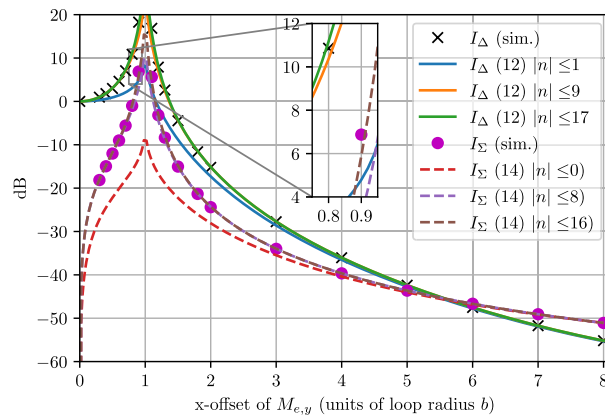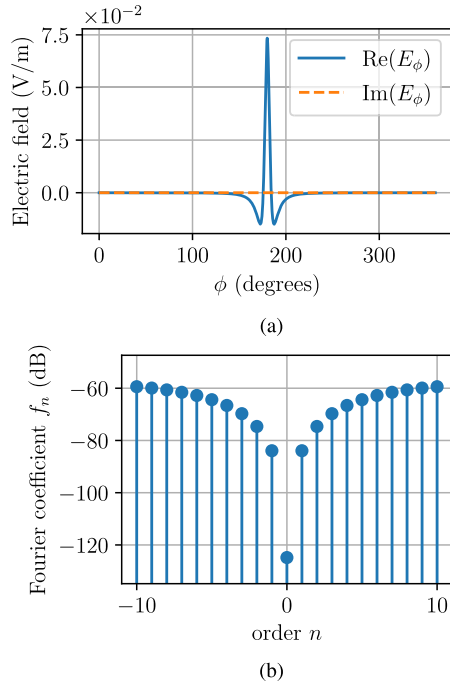

(a) x-offset
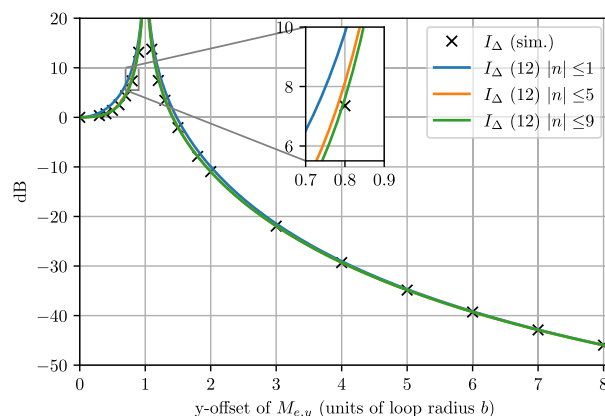
(b) y-offset.
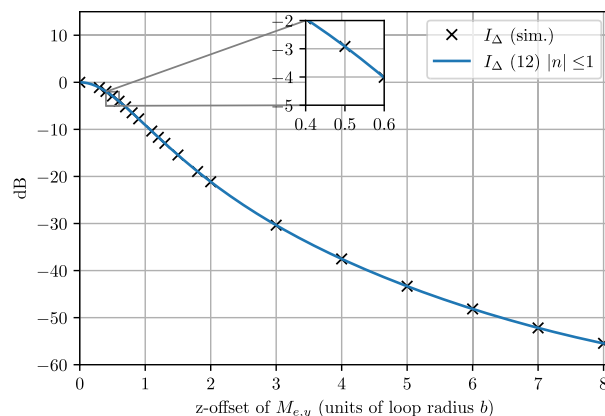
(c) z-offset.

FIGURE 3. The port currents of a dual-loaded loop centered in xy-plane obtained from theory and simulation of a y-directed electric dipole as a function of dipole offsets along the: (a) x-axis, (b) y-axis, and (c) z-axis. The theoretical currents were obtained using (12) and (14), respectively, with (5) and (39). The results in (b) and (c) exclude I_Σ as it is insignificant (at least 80 dB below the shown data). Plots are normalized to the response when the dipole is at the center of the loop. The port impedances were $Z_L = 315$ Ω.

as shown in Fig. 4. For this special-case configuration, more Fourier coefficient terms must be included to accurately model the port currents.

(a)

(b)

FIGURE 4. Example of the loop tangential electric field E_ϕ when an electric dipole is offset $0.9b$ from the center of the loop along the x-axis. (a) E_ϕ along the loop of radius $kb = 0.1$ rad, and (b) the corresponding Fourier series coefficients.

B. MAGNETIC DIPOLE SOURCE

Fig. 7 shows the simulation model for a small magnetic dipole source, using a similar dual-loaded loop configuration as described in Section IV-A. The magnetic dipole, with an electrical area 2×10^{-7} rad·m, was oriented with its moment vector (normal vector to the dual-loaded loop) in the z-direction and was shifted along the Cartesian coordinate axes.

1) VERIFICATION OF THE THEORETICAL PORT CURRENTS FROM A MAGNETIC DIPOLE

Fig. 8 shows the matching between the theoretical and simulated I_Δ and I_Σ port currents as the magnetic dipole is shifted along the Cartesian axes. The theoretical I_Δ and I_Σ currents were calculated using Python implementing (12) and (14), respectively, with (5) and (51).

In contrast to the electric dipole case, very few loop current Fourier series coefficients are required to accurately model the port currents from a magnetic dipole. Fig. 8 shows that to achieve accurate current estimates for I_Σ, only the first-order Fourier coefficient I_0 is required. The worst case convergence was for the weaker I_Δ when the magnetic dipole was shifted along the x-axis, requiring an additional Fourier coefficient order, i.e., $|n| = 3$, to model the loop port current accurately.

2) EVALUATION OF FIRST-ORDER PORT CURRENT ESTIMATES FROM A MAGNETIC DIPOLE

As the magnetic dipole was shifted in the simulation model, the port currents and E_ϕ along the loop were collected.


(a) x-offset
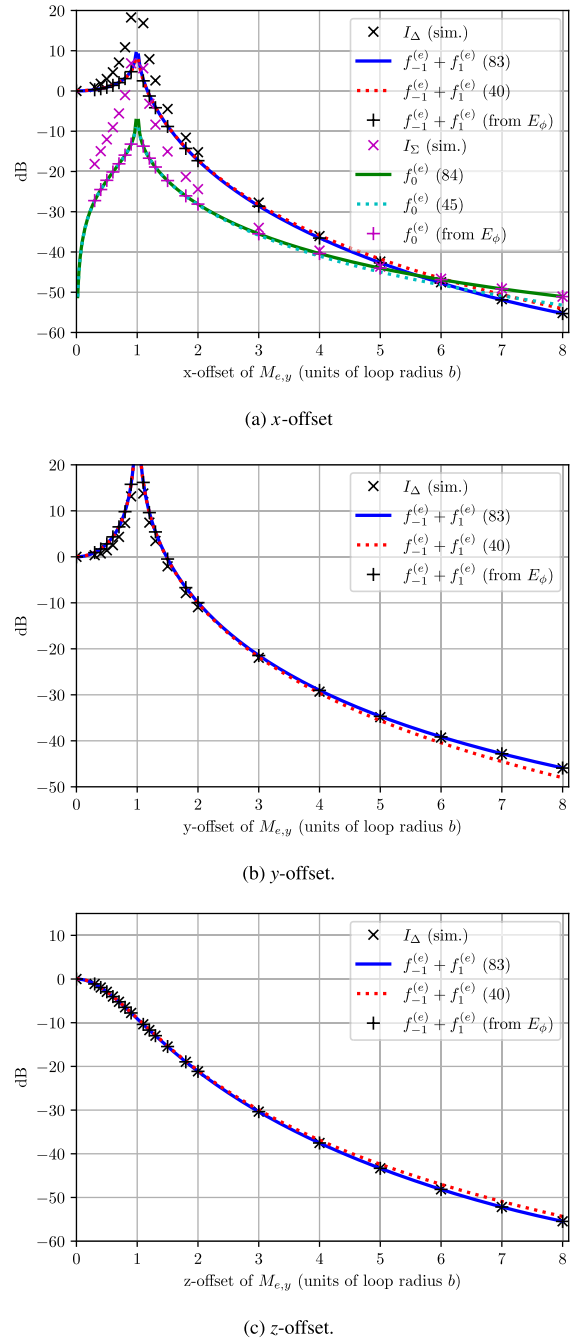
(b) y-offset.

(c) z-offset.

FIGURE 5. Theory and simulation of a y-directed electric dipole coupling to a dual-loaded loop centered xy-plane, as a function of dipole offsets along the: (a) x-axis, (b) y-axis, and (c) z-axis. The expressions (83) and (84) are accurate over all the offsets. The leading term approximations, (40) and (45), match the response when the offset is small and gradually degrades as the offset increases. The current estimates (13) and (15) are seen to degrade when the dipole is near the loop. The results are normalized to the value at the origin. The results in (b) and (c) exclude $f_0^{(e)}$ and I_Σ as they are insignificant (at least 80 dB below the shown data). The port impedances were $Z_L = 315$ Ω.

The Fourier series for E_ϕ was used to verify the first-order Fourier coefficients predicted by the new theory.

(a) *x*-offset

(b) *y*-offset

(c) *z*-offset
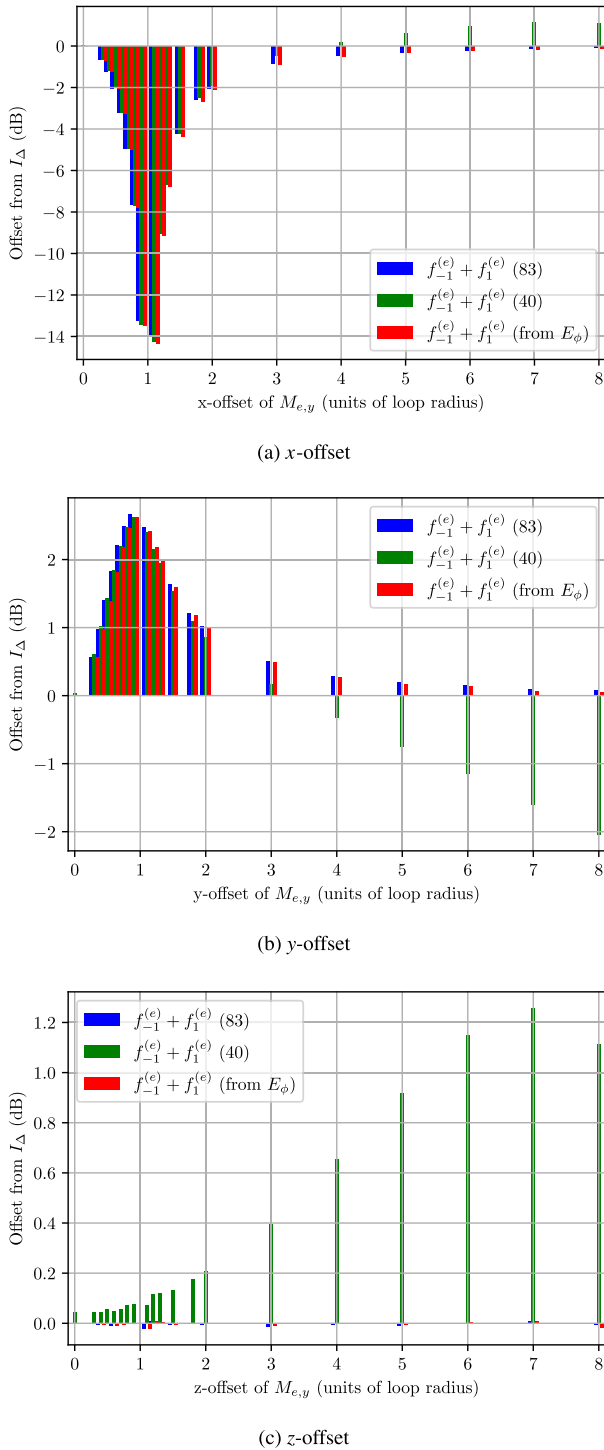
FIGURE 6. Difference between the simulated I_Δ and its approximation (13) using Fourier coefficients from either (83), (40), or E_ϕ determined from the simulated field.

Fig. 9 compares the first-order Fourier series coefficients of the port current obtained through simulation and theory for the magnetic dipole source. As was seen for the electric dipole
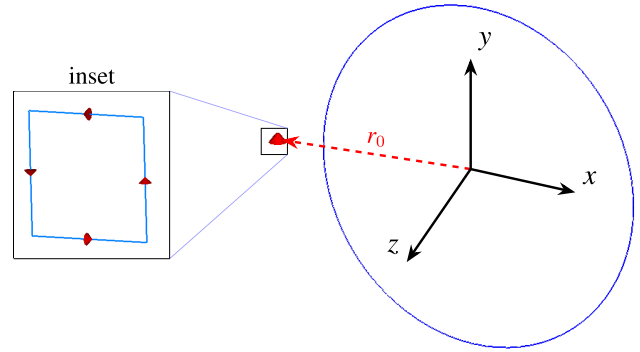
FIGURE 7. Model to determine the simulated Fourier series coefficients of E_ϕ along a dual-loaded loop with an electrical radius of $kb = 0.1$ rad. A *z*-directed magnetic dipole, of electrical area of 2×10^{-7} rad·m, is shifted by the vector r_0.

case, excellent agreement is observed between the derived Fourier coefficients and the full expressions for the loop-mode (85) and dipole-mode (86) over the dipole offset range. Small kR approximations (52) and (53) are accurate for small dipole offsets, being within 1 dB when $kR < 0.5$, and degrade as the offsets increase.

Fig. 9 also shows the modelling of port currents using the first-order Fourier series estimates (13) and (15). Unlike in the electric dipole case, there is excellent agreement across all of the offsets, even when the magnetic dipole approaches the loop. This is shown in Fig. 10, where the first-order estimates I_0 are compared with the simulated port current I_Σ. The estimates for I_Σ that use the full expression (85) are within 0.3 dB across the offset range.

V. DISCUSSION

The results show that care must be taken if I_Δ is approximated when an electric dipole source is near the loop, a condition that requires a large number of current Fourier series coefficients to model the port currents accurately. However, for offsets either near the center or away from the loop, e.g., $kr_0 > 0.3$, the first-order estimates yield accurate results – i.e., I_Δ estimated from (13) with (83), and I_Σ estimated from (15) with (84).

Unlike the case for an electric dipole source, the first-order current estimates provide accurate results for a magnetic dipole source across all offsets – i.e., when I_Σ is estimated from (15) with (85) and I_Δ is estimated from (13) with (86). When the offset is small, $kr_0 < 0.3$, the simpler estimates (52) and (53) can be used.

Although the closed-form expressions for the loop current Fourier coefficients may appear complicated, they comprise a summation of Gaussian hypergeometric functions that are extremely quick to calculate. Even the most complicated expression (83) takes less than 5 ms on a low-end personal computer (e.g., Intel® Core™ i5-3470), whereas a method of moments simulation can take on the order of minutes for
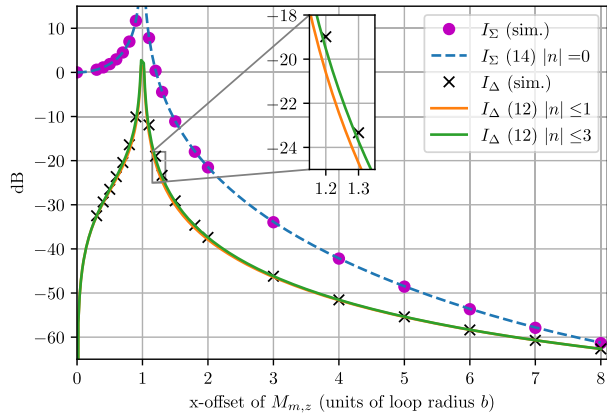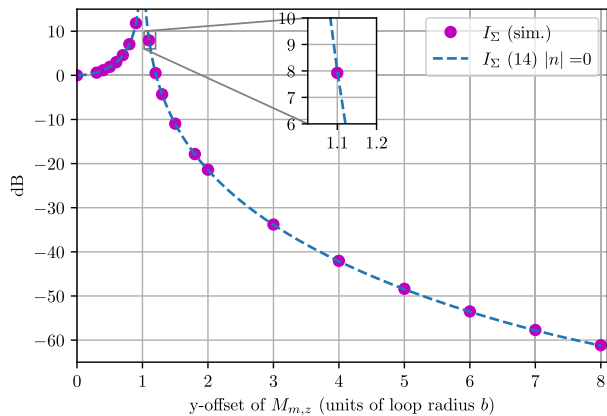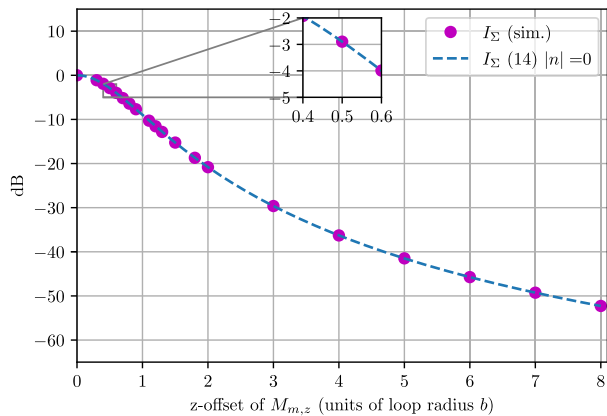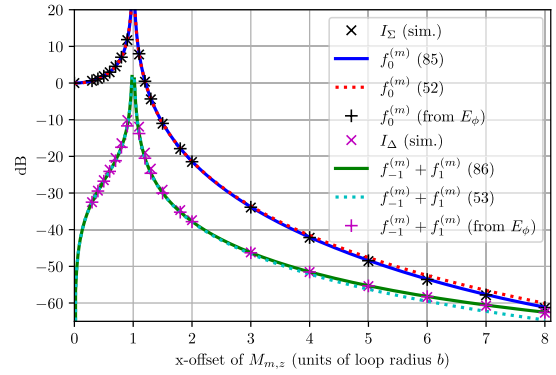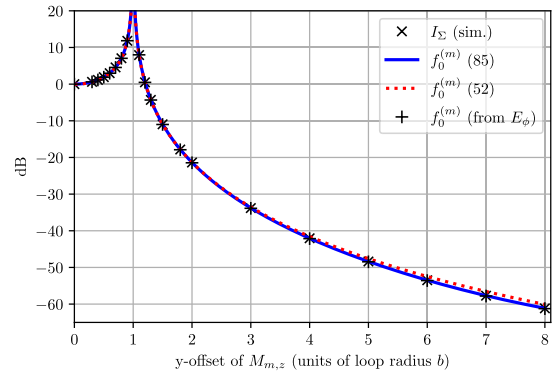
FIGURE 8. The port currents of a dual-loaded loop centered in *xy*-plane obtained from theory and simulation of a *z*-directed magnetic dipole as a function of dipole offsets along the: (a) *x*-axis, (b) *y*-axis, and (c) *z*-axis. The theoretical currents were obtained using (12) and (14), respectively, with (5) and (51). The results in (b) and (c) exclude I_Δ as it is insignificant (at least 80 dB below the shown data). Plots are normalized to the response when the dipole is at the center of the loop. The port impedances were $Z_L = 315$ Ω.

FIGURE 9. Theory and simulation of a *z*-directed magnetic dipole coupling to a dual-loaded loop centered *xy*-plane, as a function of dipole offsets along the: (a) *x*-axis, (b) *y*-axis, and (c) *z*-axis. The expressions (85) and (86) are accurate across offsets. The leading term approximations, (52) and (53), match the response when the offset is small and gradually degrades as the offset increases. The current estimates (13) and (15) are accurate for most dipole offsets, with small degradation occurring when the dipole is near the dual-loaded loop. The results are normalized to the value at the origin. The results in (b) and (c) exclude $f_{-1}^{(m)} + f_{-1}^{(m)}$ and I_Δ as they are insignificant (at least 80 dB below the shown data). The port impedances were $Z_L = 315$ Ω.
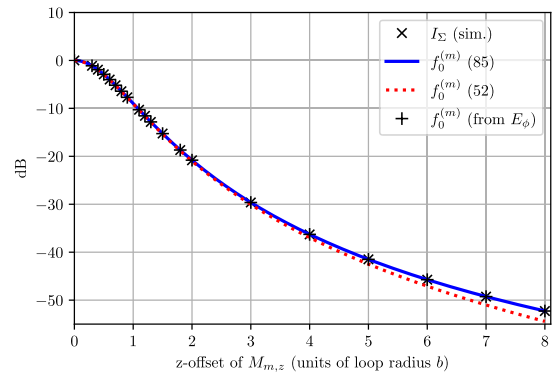
each configuration. It is noted that the Fourier coefficients can also be determined by the evaluating the integrals of the tangential electric field (39) and (51), however, these require
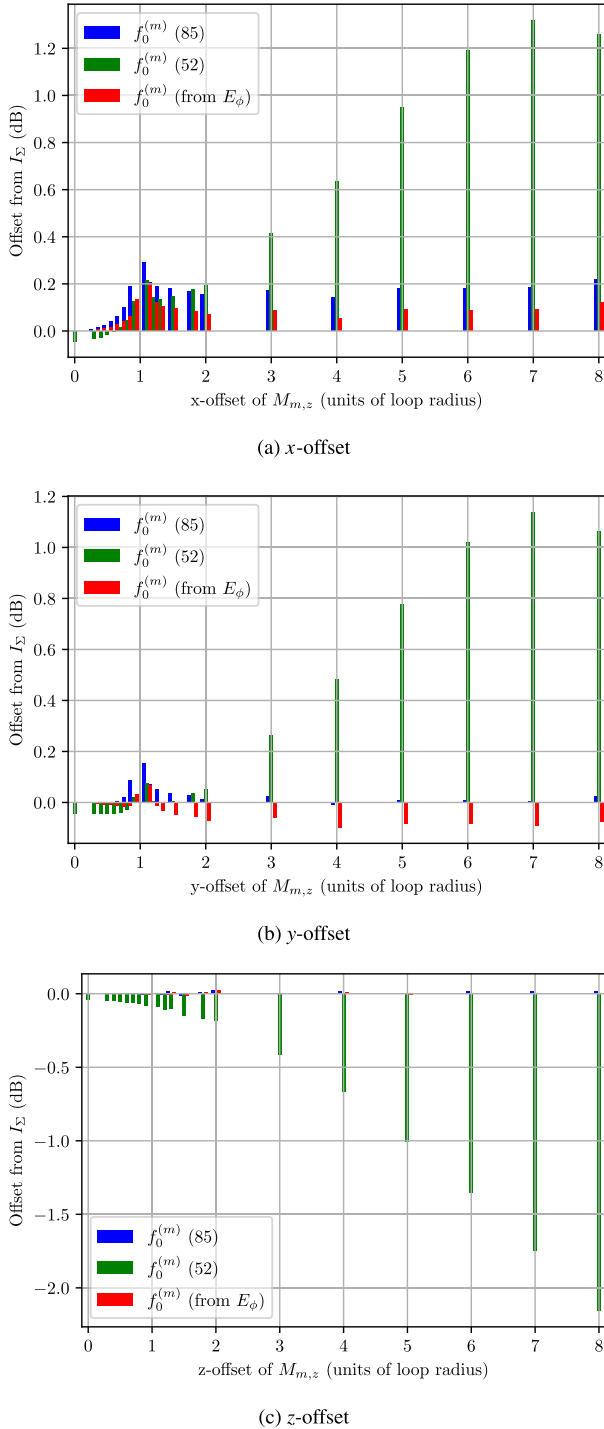
significantly more time to evaluate than the hypergeometric closed-form expressions. Additionally, these closed-form expressions offer a benchmark for verifying such integral evaluations.

(a) x-offset

(b) y-offset

(c) z-offset

FIGURE 10. Difference between the simulated I_Σ and first-order Fourier series coefficient approximation (15) using $f_0^{(m)}$ determined from (85), (52), or E_ϕ determined from the simulated field.

VI. CONCLUSION

The three-loop antenna system comprises three co-located, orthogonally oriented, dual-loaded loops. Motivated by using a three-loop antenna system for near-field detection of all six field components, the existing theory of the single dual-loaded loop is extended in this study. New expressions

are developed for the responses to electric and magnetic dipole sources that are offset from the center of the loop, and are verified for a radial range of up to eight times the loop radius. The expressions are verified by simulation for a specific loop configuration of loop: wire electrical radius $ka = 2 \times 10^{-3}$ rad, loop radius $kb = 0.1$ rad, and electric dipole length 1.2×10^{-3} rad and magnetic dipole from a square loop of electrical area 2×10^{-7} rad·m. For both electric and magnetic dipoles, closed-form approximations for the first-order Fourier current expansion are determined and offer a fast calculation benchmark for the loop port currents. For the magnetic dipole case, the accuracy is excellent. For an electric dipole, the accuracy degrades only when it is close to, and aligned with, one of the feed ports owing to the truncation of the higher Fourier terms.

APPENDIX. FOURIER COEFFICIENTS

To evaluate the integrals for the Fourier series coefficients of the tangential electric field across a dual-loaded loop, the integration argument is extended to a complex argument via $w = e^{j\phi}$. The exponential term in (28) and (48) is expanded using [19], [20], [31], [32], [33, (10.1.39-40)]

$$e^{j\sqrt{\hat{R}^2 - 2k^2 b(x_0 \cos \phi + y_0 \sin \phi)}}$$

$$= \sum_{\ell=0}^{\infty} \frac{(k^2 b)^\ell}{\ell!} \frac{h_{\ell-1}^{(1)}(\hat{R})}{\hat{R}^{\ell-1}} (x_0 \cos \phi + y_0 \sin \phi)^\ell, \quad (54)$$

$$= \sum_{\ell=0}^{\infty} \frac{(k^2 b w_0^*)^\ell}{\ell!} \frac{h_{\ell-1}^{(1)}(\hat{R})}{\hat{R}^{\ell-1}} \frac{(w^2 + e^{j2\theta_0})^\ell}{2^\ell w^\ell}, \quad (55)$$

where $h_n^{(1)}$ is the spherical Hankel function of the first kind of order n and

$$w_0 = x_0 + jy_0 = |w_0| e^{j\theta_0}. \quad (56)$$

The spherical Hankel function can be expressed as a summation [33, (10.1.16)],

$$h_{\ell-1}^{(1)}(\hat{R}) = j^{-\ell} \hat{R}^{-1} e^{j\hat{R}} \sum_{k=0}^{\ell-1} \frac{(\ell-1+k)!}{k!(\ell-1-k)!} (-2j\hat{R})^{-k}, \ \ell \geq 1. \quad (57)$$

As $\hat{R}$ approaches zero, (57) is well approximated by the highest orders of $\hat{R}^{-1}$. For the dominant modes, using only the highest order is sufficient,

$$h_{\ell-1}^{(1)}(\hat{R}) \to -j \frac{e^{j\hat{R}}}{\hat{R}^\ell} \frac{(2(\ell-1))!}{(\ell-1)! 2^{\ell-1}}, \quad (58)$$

$$= \binom{1/2}{\ell} (-1)^\ell \ell! 2^\ell \frac{j e^{j\hat{R}}}{\hat{R}^\ell}, \ \text{as} \ \hat{R} \to 0, \ \ell \geq 1, \quad (59)$$

where for any complex arguments x and y [33, (6.1.21)]

$$\binom{x}{y} = \frac{\Gamma(x+1)}{\Gamma(y+1)\Gamma(x+y+1)}, \quad (60)$$

and $\Gamma(\cdot)$ is the gamma function. The above approximation of the spherical Hankel function is the only approximation in the

derivations below. When investigating the accuracy of weaker modes, specifically the loop-mode for an electric dipole, the two highest reciprocal order terms are necessary in (57) to well approximate the non-dominant mode [34],

$$h_{\ell-1}^{(1)}(\hat{R}) \rightarrow -j\frac{e^{j\hat{R}}}{\hat{R}^\ell}\frac{(2(\ell-1))!}{(\ell-1)!2^{\ell-1}}(1-j\hat{R}) \quad (61)$$

$$= \binom{1/2}{\ell}(-1)^\ell \ell! 2^\ell \frac{e^{j\hat{R}}}{\hat{R}^\ell}(1-j\hat{R}), \text{ as } \hat{R} \rightarrow 0, \ell \geq 2. \quad (62)$$

Using the Hankel function approximation of (59), the complex exponential (55) is

$$e^{j\sqrt{\hat{R}^2-2k^2b(x_0\cos\phi+y_0\sin\phi)}} \approx$$

$$e^{j\hat{R}}\left[(1-j\hat{R})+j\hat{R}\sum_{\ell=0}^{\infty}\binom{1/2}{\ell}\alpha^\ell\frac{(w^2+e^{j2\theta_0})^\ell}{w^\ell}\right], \quad (63)$$

where

$$\alpha = -bw_0^*/R^2. \quad (64)$$

It can shown [34] that (63) is also accurate for large offsets, i.e., $r_0 \gg b$, so the derived results based on (63) will be accurate except near the loop.

The denominators in (28) and (48) can be expanded using the binomial expansion [33, (3.7.22)] as

$$\left[\hat{R}^2 - 2k^2b(x_0\cos\phi+y_0\sin\phi)\right]^\xi =$$

$$\hat{R}^{2\xi}\sum_{m=0}^{\infty}\binom{\xi}{m}\alpha^m\frac{(w^2+e^{j2\theta_0})^m}{w^m}, \quad (65)$$

where ξ is a rational number.

The infinite summations are handled below.

A. ELECTRIC DIPOLE FOURIER COEFFICIENTS

The expression for the Fourier coefficients (39) for the tangential electric field on a loop from an electric dipole source is expanded using (63) and (65)

$$f_n^{(e)} \approx$$

$$\frac{\eta k^4}{8\pi^2}\oint_{C_1} dw\, w^{n-1}\left(\hat{R}^{-3}\sum_{m=0}^{\infty}\binom{-3/2}{m}\alpha^m\frac{(w^2+e^{j2\theta_0})^m}{w^m}\times\right.$$

$$\left(B'\frac{w^2-1}{2jw}+C'\frac{w^2+1}{2w}+D\frac{w^4-1}{2jw^2}+E\frac{w^4+1}{2w^2}-\frac{3F}{5}\right)$$

$$+\left(\hat{R}^{-5}\sum_{m=0}^{\infty}\binom{-5/2}{m}\alpha^m\frac{(w^2+e^{j2\theta_0})^m}{w^m}\right.$$

$$\left.-j\hat{R}^{-4}\sum_{m=0}^{\infty}\binom{-2}{m}\alpha^m\frac{(w^2+e^{j2\theta_0})^m}{w^m}\right)\times$$

$$\left(B\frac{we^2-1}{2jw}+C\frac{w^2+1}{2w}+D\frac{w^4-1}{2jw^2}+E\frac{w^4+1}{2w^2}+F\right)\right)$$

$$\left.\times\left(e^{j\hat{R}}(1-j\hat{R})+je^{j\hat{R}}\hat{R}\sum_{\ell=0}^{\infty}\binom{1/2}{\ell}\alpha^\ell\frac{(w^2+e^{j2\theta_0})^\ell}{w^\ell}\right),\right.$$

$$(66)$$

$$= \frac{\eta e^{j\hat{R}}}{8\pi k R^5}\left[B\left[S_{n,0,0}-S_{n,2,0}+j\hat{R}(S_{n,0,\infty}-S_{n,2,\infty})\right.\right.$$

$$-S_{n,0,0}+S_{n,2,0}-Q_{n,0,0}+Q_{n,2,0}+\hat{R}^2(Q_{n,0,\infty}$$

$$-Q_{n,2,\infty}-Q_{n,0,0}+Q_{n,2,0}-T_{n,0,0}+T_{n,2,0})$$

$$\left.-j\hat{R}^3(T_{n,0,\infty}-T_{n,2,\infty}-T_{n,0,0}+T_{n,2,0})\right]$$

$$+jC\left[S_{n,0,0}+S_{n,2,0}+j\hat{R}(S_{n,0,\infty}+S_{n,2,\infty}-S_{n,0,0}\right.$$

$$-S_{n,2,0}-Q_{n,0,0}-Q_{n,2,0})+\hat{R}^2(Q_{n,0,\infty}+Q_{n,2,\infty}$$

$$-Q_{n,0,0}-Q_{n,2,0}-T_{n,0,0}-T_{n,2,0})$$

$$\left.-j\hat{R}^3(T_{n,0,\infty}+T_{n,2,\infty}-T_{n,0,0}-T_{n,2,0})\right]$$

$$+D\left[S_{n,-1,0}-S_{n,3,0}+j\hat{R}(S_{n,-1,\infty}-S_{n,3,\infty}-S_{n,-1,0}\right.$$

$$+S_{n,3,0}-Q_{n,-1,0}+Q_{n,3,0})+\hat{R}^2(Q_{n,-1,\infty}-Q_{n,3,\infty}$$

$$-Q_{n,-1,0}+Q_{n,3,0}+T_{n,-1,0}-T_{n,3,0})$$

$$\left.+j\hat{R}^3(T_{n,-1,\infty}-T_{n,3,\infty}-T_{n,-1,0}+T_{n,3,0})\right]$$

$$+jE\left[S_{n,-1,0}+S_{n,3,0}+j\hat{R}(S_{n,-1,\infty}+S_{n,3,\infty}-S_{n,-1,0}\right.$$

$$-S_{n,3,0}-Q_{n,-1,0}-Q_{n,3,0})+\hat{R}^2(Q_{n,-1,\infty}+Q_{n,3,\infty}$$

$$-Q_{n,-1,0}-Q_{n,3,0}+T_{n,-1,0}+T_{n,3,0})$$

$$\left.+j\hat{R}^3(T_{n,-1,\infty}+T_{n,3,\infty}-T_{n,-1,0}-T_{n,3,0})\right]$$

$$+j2F\left[S_{n,1,0}+j\hat{R}(S_{n,1,\infty}-S_{n,1,0}-Q_{n,1,0})\right.$$

$$+\hat{R}^2(Q_{n,1,\infty}-Q_{n,1,0}-\frac{3}{5}T_{n,1,0})$$

$$\left.-j\frac{3}{5}\hat{R}^3(T_{n,1,\infty}-T_{n,1,0})\right]$$

$$-2x_0\mathbf{m}_e\cdot\mathbf{r}_0\left[\hat{R}^2(T_{n,0,0}-T_{n,2,0})\right.$$

$$\left.+j\hat{R}^3(T_{n,0,\infty}-T_{n,2,\infty}-T_{n,0,0}+T_{n,2,0})\right]$$

$$+2jy_0\mathbf{m}_e\cdot\mathbf{r}_0\left[\hat{R}^2(T_{n,0,0}+T_{n,2,0})\right.$$

$$\left.\left.+j\hat{R}^3(T_{n,0,\infty}+T_{n,2,\infty}-T_{n,0,0}-T_{n,2,0})\right]\right], \quad (67)$$

where

$$S_{n,p,q} = \sum_{m=0}^{\infty}\sum_{\ell=0}^{q}\binom{-5/2}{m}\binom{1/2}{\ell}\alpha^{m+\ell}g(\ell,m,n,p), \quad (68)$$

$$Q_{n,p,q} = \sum_{m=0}^{\infty}\sum_{\ell=0}^{q}\binom{-2}{m}\binom{1/2}{\ell}\alpha^{m+\ell}g(\ell,m,n,p), \quad (69)$$

$$T_{n,p,q} = \sum_{m=0}^{\infty}\sum_{\ell=0}^{q}\binom{-3/2}{m}\binom{1/2}{\ell}\alpha^{m+\ell}g(\ell,m,n,p), \quad (70)$$

$$g(\ell,m,n,p) = \frac{1}{2\pi j}\oint_{C_1}\frac{(w^2+e^{j2\theta_0})^{m+\ell}}{w^{m+\ell-n+p}}dw, \quad (71)$$

and the contour C_1 in the complex plane is the unit circle.

The Residue theorem can be used to perform the complex integrations (71). The integrand is analytic except at the poles at the origin, and is solved using Cauchy's integral formula,

$$\frac{1}{2\pi j}\oint_{C_1}\frac{\tilde{g}(w)}{w^{q+1}}dw = \frac{\tilde{g}^{(q)}(0)}{q!}, \quad q \geq 0, \quad (72)$$

where, from (71),

$$\tilde{g}(w) = (w^2+e^{j2\theta_0})^{m+\ell}, \quad (73)$$

and this can be expanded in a binomial series [33, (3.7.22)] as

$$\tilde{g}(w) = \sum_{i=0}^{m+\ell} \binom{m+\ell}{i} w^{2(m+\ell-i)} e^{j2i\theta_0}. \qquad (74)$$

The qth derivative of $\tilde{g}(w)$ is

$$\tilde{g}^{(q)}(w) = \sum_{i=0}^{m+\ell-\lceil \frac{q}{2} \rceil} \binom{m+\ell}{i} \times \left[\prod_{r=0}^{q-1} 2(m+\ell-i) - r \right] w^{2(m+\ell-i)-q} e^{j2i\theta_0}, \qquad (75)$$

where $\lceil \cdot \rceil$ rounds up to the nearest integer. When evaluated at $w = 0$,

$$\frac{\tilde{g}^{(q)}(0)}{q!} = \binom{m+\ell}{q/2} e^{j(m+\ell-\frac{q}{2})2\theta_0}, \qquad (76)$$

if q is even and $0 \leq q \leq 2(m+\ell)$, otherwise it is zero.

Using (72) and (76), the arithmetic function (71) reduces to

$$g(\ell, m, n, p) = \binom{m+\ell}{(m+\ell-n+p-1)/2} e^{j(m+\ell+n-p+1)\theta_0}, \qquad (77)$$

if $m+\ell-n+p$ is odd and $0 \leq m+\ell-n+p-1 \leq 2(m+\ell)$, otherwise it is zero.

B. MAGNETIC DIPOLE FOURIER COEFFICIENTS

The expression for the Fourier coefficients (51) for the tangential electric field on a loop from a magnetic dipole source is expanded as a summation of terms using (63) and (65)

$$f_n^{(m)} \approx \frac{k^4 \eta}{8\pi^2 j} \times$$

$$\oint_{C_1} dw w^{n-1} \left[bm_{m,z} + G\frac{w^2-1}{2jw} + H\frac{w^2+1}{2w} \right] \times$$

$$\left(\hat{R}^{-2} \sum_{p=0}^{\infty} \binom{-1}{p} \alpha^p \frac{(w^2+e^{j2\theta_0})^p}{w^p} \right. \qquad (78)$$

$$\left. +j\hat{R}^{-3} \sum_{m=0}^{\infty} \binom{-3/2}{m} \alpha^m \frac{(w^2+e^{j2\theta_0})^m}{w^m} \right) \times$$

$$\left(e^{j\hat{R}}(1-j\hat{R}) + je^{j\hat{R}}\hat{R} \sum_{\ell=0}^{\infty} \binom{1/2}{\ell} \alpha^\ell \frac{(w^2+e^{j2\theta_0})^\ell}{w^\ell} \right),$$

$$= \frac{k\eta e^{j\hat{R}}}{j8\pi R^3} \left(j\hat{R}^2 \left[j2bm_{m,z}U_{n,1,\infty} + (G+jH)U_{n,0,\infty} \right. \right.$$

$$\left. - (G-jH)U_{n,2,\infty} \right] - \hat{R} \left[j2bm_{m,z}T_{n,1,\infty} \right. \qquad (79)$$

$$\left. + (G+jH)T_{n,0,\infty} - (G-jH)T_{n,2,\infty} \right]$$

$$+ \hat{R}(1-j\hat{R}) \left[j2bm_{m,z}U_{n,1,0} + (G+jH)U_{n,0,0} \right.$$

$$\left. - (G-jH)U_{n,2,0} \right] + j(1-j\hat{R}) \left[j2bm_{m,z}T_{n,1,0} \right.$$

$$\left. + (G+jH)T_{n,0,0} - (G-jH)T_{n,2,0} \right] \right),$$

where

$$U_{n,p,q} = \sum_{m=0}^{\infty} \sum_{\ell=0}^{q} \binom{-1}{m} \binom{1/2}{\ell} \alpha^{m+\ell} g(\ell, m, n, p). \qquad (80)$$

C. FIRST-ORDER FOURIER COEFFICIENTS

For centrally located dipole sources, the dominant modes tend to be the dipole-mode given by (13), i.e., $f_{-1} + f_1$, and the loop-mode given by (15), i.e., f_0. These Fourier coefficients were determined using (67) and (78). When $n = \pm 1$ and $n = 0$, each summation (68)-(70) and (80) can be expressed [34] in terms of the Gaussian hypergeometric function using (77) and the Chu-Vandermonde identity [33, (24.1.1.II.B)]

$$\sum_{k=0}^{n} \binom{s}{k} \binom{t}{n-k} = \binom{s+t}{n}. \qquad (81)$$

Each summation term of (68)-(70) and (80), using (81), is of the form (for different values of the parameter p and be such that either $m = n$ or $m = 0$),

$$\sum_{t=0}^{\infty} \binom{-p}{2t+n} \binom{2t+n}{t+m} x^t$$

$$= \sum_{t=0}^{\infty} \frac{(-p)^{2t+n}}{(2t+n)!} \frac{(2t+n)!}{(t+n)!} \frac{x^t}{t!},$$

$$= (-1)^n \sum_{t=0}^{\infty} \frac{p^{\overline{n}}(p+n)^{\overline{2t}}}{(t+n)!} \frac{x^t}{t!},$$

$$= (-1)^n p^{\overline{n}} \sum_{t=0}^{\infty} \frac{(2(\frac{n}{2}+\frac{p}{2}))^{\overline{2t}}}{1^{\overline{t+n}}} \frac{x^t}{t!},$$

$$= (-1)^n \frac{p^{\overline{n}}}{n!} \sum_{t=0}^{\infty} \frac{(\frac{p}{2}+\frac{n}{2})^{\overline{t}}(\frac{p+1}{2}+\frac{n}{2})^{\overline{t}}}{(1+n)^{\overline{t}}} \frac{(4x)^t}{t!},$$

$$= (-1)^n \frac{p^{\overline{n}}}{n!} \, {}_2F_1\left(\frac{p+n}{2}, \frac{p+n+1}{2}; n+1; 4x \right), \qquad (82)$$

where $(x)^{\overline{n}} = \prod_{k=0}^{n-1}(x+k)$ and $(x)^{\underline{n}} = \prod_{k=0}^{n-1}(x-k)$.

Using (67) and (82), the full expression of the dipole-mode from an electric dipole source is [34]

$$f_{-1}^{(e)} + f_1^{(e)} \approx \frac{j\eta b^2 e^{j\hat{R}}}{4\pi kR^7} \left\{ (c-\epsilon) \left[(1-j\hat{R}) \, {}_2F_1\left(\frac{5}{4}, \frac{7}{4}; 1; \zeta \right) \right. \right.$$

$$\left. -\hat{R}^2 \frac{1}{(1-\zeta)^{3/2}} + j\hat{R}^3 \left({}_2F_1\left(\frac{3}{4}, \frac{5}{4}; 1; \zeta \right) - \frac{1}{\sqrt{1-\zeta}} \right) \right]$$

$$-\left(d+\frac{\zeta c}{4} \right) \left[(1-j\hat{R})\frac{35}{8} \, {}_2F_1\left(\frac{9}{4}, \frac{11}{4}; 3; \zeta \right) \right.$$

$$- 3\hat{R}^2 \, {}_2F_1\left(2, \frac{5}{2}; 3; \zeta \right) + j\hat{R}^3 \left(\frac{15}{8} \, {}_2F_1\left(\frac{7}{4}, \frac{9}{4}; 3; \zeta \right) \right.$$

$$\left. - {}_2F_1\left(\frac{3}{2}, 2; 3; \zeta \right) \right) \right] - \frac{\zeta \epsilon}{8} \left[(1-j\hat{R})\frac{5}{2} \, {}_2F_1\left(\frac{7}{4}, \frac{9}{4}; 2; \zeta \right) \right.$$

$$+ \hat{R}^2 \left(3 \, _2F_1 \left(\frac{5}{4}, \frac{7}{4}; 2; \zeta \right) - \frac{2}{(1-\zeta)^{3/2}} \right)$$

$$-j\hat{R}^3 \left(\frac{3}{2} \, _2F_1 \left(\frac{5}{4}, \frac{7}{4}; 2; \zeta \right) - \, _2F_1 \left(1, \frac{3}{2}; 2; \zeta \right) \right) \Big]$$

$$- \frac{\zeta d}{8} \left[(1-j\hat{R}) \frac{105}{16} \, _2F_1 \left(\frac{11}{4}, \frac{13}{4}; 4; \zeta \right) \right.$$

$$+ \hat{R}^2 \left(\frac{35}{8} \, _2F_1 \left(\frac{9}{4}, \frac{11}{4}; 4; \zeta \right) - 4 \, _2F_1 \left(\frac{5}{2}, 3; 4; \zeta \right) \right)$$

$$+ j\hat{R}^3 \left(\, _2F_1 \left(2, \frac{5}{2}; 4; \zeta \right) - \frac{35}{16} \, _2F_1 \left(\frac{9}{4}, \frac{11}{4}; 4; \zeta \right) \right) \Big]$$

$$- 5 \, x_0 (\mathbf{m}_e \times \mathbf{r}_0)_z \left[(1-j\hat{R}) \frac{5}{2} \, _2F_1 \left(\frac{7}{4}, \frac{9}{4}; 2; \zeta \right) \right.$$

$$+ \hat{R}^2 \left(\frac{3}{5} \, _2F_1 \left(\frac{5}{4}, \frac{7}{4}; 2; \zeta \right) - \frac{2}{(1-\zeta)^{3/2}} \right)$$

$$+ j\frac{3}{5}\hat{R}^3 \left(\frac{3}{2} \, _2F_1 \left(\frac{5}{4}, \frac{7}{4}; 2; \zeta \right) - \, _2F_1 \left(1, \frac{3}{2}; 2; \zeta \right) \right) \Big]$$

$$+ \hat{R}^2 \frac{2c}{3} \left[(1-j\hat{R}) \left(\, _2F_1 \left(\frac{3}{4}, \frac{5}{4}; 1; \zeta \right) \right. \right.$$

$$- \frac{15}{32} \zeta \, _2F_1 \left(\frac{7}{4}, \frac{9}{4}; 3; \zeta \right) \Big)$$

$$-j\hat{R} \left(\frac{\zeta}{4} \, _2F_1 \left(\frac{3}{2}, 2; 3; \zeta \right) - \frac{1}{\sqrt{1-\zeta}} \right) \Big] \Big\}. \qquad (83)$$

The full expression of the loop-mode from an electric dipole source, when using the two highest reciprocal order terms for the Hankel function expansion (62) [34], is

$$f_0^{(e)} \approx \frac{j\eta bk e^{j\hat{R}}}{8\pi R^3} (\mathbf{m}_e \times \mathbf{r}_0)_z \left\{ \frac{4}{\zeta} \left((\zeta - 5) \, _2F_1 \left(\frac{3}{4}, \frac{5}{4}; 1; \zeta \right) \right. \right.$$

$$-5(\zeta-1) \, _2F_1 \left(\frac{3}{4}, \frac{9}{4}; 1; \zeta \right) \Big) - j\hat{R} \left(\frac{15}{16} \zeta \, _2F_1 \left(\frac{7}{4}, \frac{9}{4}; 3; \zeta \right) \right.$$

$$- 2 \, _2F_1 \left(\frac{3}{4}, \frac{5}{4}; 1; \zeta \right) + \frac{1}{\sqrt{1-\zeta}} \Big)$$

$$+ \hat{R}^2 \frac{2}{3\zeta} \left(2(2\zeta - 5)(\zeta - 1) \, _2F_1 \left(\frac{3}{4}, \frac{5}{4}; 1; \zeta \right) \right.$$

$$- 10(\zeta - 1)^2 \, _2F_1 \left(\frac{3}{4}, \frac{9}{4}; 1; \zeta \right) - 3\sqrt{1-\zeta} + 3 \Big) \Big\}. \qquad (84)$$

(84) is a simplified results through applying Gauss' relations for contiguous hypergeometric functions [33, (15.2)] to (67). This simplified form is undefined at $\zeta = 0$ but its value can be determined through taking the limit as ζ approaches 0.

Using (78) and (82), the full expression of the loop-mode from a magnetic dipole source is [34]

$$f_0^{(m)} \approx \frac{jkb\eta e^{j\hat{R}}}{4\pi R^3} \left\{ m_{m,z} \left[(1-jR) \, _2F_1 \left(\frac{3}{4}, \frac{5}{4}; 1; \zeta \right) \right. \right.$$

$$+ \hat{R}^2 \left(\, _2F_1 \left(\frac{1}{4}, \frac{3}{4}; 1; 4\beta^2 \right) - \frac{1}{\sqrt{1-\zeta}} \right) \Big]$$

$$+ \frac{((\mathbf{m}_m \times \mathbf{r}_0) \times \mathbf{r}_0)_z}{2R^2} \left[3(1-j\hat{R}) \, _2F_1 \left(\frac{5}{4}, \frac{7}{4}; 2; \zeta \right) \right.$$

$$+\hat{R}^2 \left(\, _2F_1 \left(\frac{3}{4}, \frac{5}{4}; 2; \zeta \right) - 2 \, _2F_1 \left(1, \frac{3}{2}; 2; \zeta \right) \right) \Big] \Big\}. \qquad (85)$$

Finally, the full expression of the dipole-mode from a magnetic dipole source is [34]

$$f_{-1}^{(m)} + f_1^{(m)} \approx \frac{jkb^2 \eta e^{jkR}}{4\pi R^5} \times$$

$$\left\{ x_0 m_{m,z} \left[3(1-j\hat{R}) \, _2F_1 \left(\frac{5}{4}, \frac{7}{4}; 2; \zeta \right) \right. \right.$$

$$+ \hat{R}^2 \left(\, _2F_1 \left(\frac{3}{4}, \frac{5}{4}; 2; \zeta \right) - 2 \, _2F_1 \left(1, \frac{3}{2}; 2; \zeta \right) \right) \Big]$$

$$- \frac{R^2}{b^2} (\mathbf{m}_m \times \mathbf{r}_0)_y \left[(1-j\hat{R}) \, _2F_1 \left(\frac{3}{4}, \frac{5}{4}; 1; \zeta \right) \right.$$

$$+ \hat{R}^2 \left(\, _2F_1 \left(\frac{1}{4}, \frac{3}{4}; 1; \zeta \right) - \frac{1}{\sqrt{1-\zeta}} \right) \Big]$$

$$+ \frac{3}{8R^2} \left((\mathbf{m}_m \times \mathbf{r}_0)_x 2x_0 y_0 + (\mathbf{m}_m \times \mathbf{r}_0)_y (x_0^2 - y_0^2) \right) \times$$

$$\left[5(1-j\hat{R}) \, _2F_1 \left(\frac{7}{4}, \frac{9}{4}; 3; \zeta \right) + \hat{R}^2 \left(\, _2F_1 \left(\frac{5}{4}, \frac{7}{4}; 3; \zeta \right) \right. \right.$$

$$- \frac{8}{3} \, _2F_1 \left(\frac{3}{2}, 2; 3; \zeta \right) \Big) \Big] \Big\}. \qquad (86)$$

REFERENCES

[1] *Specification for Radio Disturbance and Immunity Measuring Apparatus and Methods—Part 1-4: Radio Disturbance and Immunity Measuring Apparatus—Antennas and Test Sites for Radiated Disturbance Measurements*, International Standard CISPR 16-1-4, The International Electrotechnical Commision (IEC), 2020.

[2] K. T. Wong, "Direction finding/polarization estimation-dipole and/or loop triad(s)," *IEEE Trans. Aerosp. Electron. Syst.*, vol. 37, no. 2, pp. 679–684, Apr. 2001.

[3] C. K. Au-Yeung and K. T. Wong, "CRB: Sinusoid-sources' estimation using collocated dipoles/loops," *IEEE Trans. Aerosp. Electron. Syst.*, vol. 45, no. 1, pp. 94–109, Jan. 2009.

[4] X. Yuan, K. T. Wong, Z. Xu, and K. Agrawal, "Various compositions to form a triad of collocated dipoles/loops, for direction finding and polarization estimation," *IEEE Sensors J.*, vol. 12, no. 6, pp. 1763–1771, Jun. 2012.

[5] J. H. Meloling, J. W. Rockway, M. P. Daly, A. R. Monges, J. C. Allen, W. R. Nielsen, P. M. McGinnis, R. B. Thompson, and N. A. Mozaffar, "A vector-sensing antenna system: A high-frequency, vector-sensing array based on the two-port loop antenna element," *IEEE Antennas Propag. Mag.*, vol. 58, no. 6, pp. 57–63, Dec. 2016.

[6] D. M. Kitavi, K. T. Wong, M. Zou, and K. Agrawal, "Lower bound of the estimation error of an emitter's direction-of-arrival/polarisation, for a collocated triad of orthogonal dipoles/loops that fail randomly," *IET Microw., Antennas Propag.*, vol. 11, no. 7, pp. 961–970, Jun. 2017.

[7] M. Kashanianfard and K. Sarabandi, "An accurate circuit model for input impedance and radiation pattern of two-port loop antennas as E- and H-probe," *IEEE Trans. Antennas Propag.*, vol. 65, no. 1, pp. 114–120, Jan. 2017.

[8] V. U. Chukwuma, B. J. Adekoya, J. E. Thomas, J. B. Emah, and R. F. Oloruntola, "On the significance of requisite criteria in detecting? Pre-earthquake ionospheric precursors: A case study of the Tohoku earthquake of March 11, 2011," *Acta Geophysica*, vol. 69, no. 4, pp. 1545–1566, Aug. 2021.

[9] C. G. Hynes and R. G. Vaughan, "Considerations on the use of three-loop antenna systems for biomedical applications," in *Proc. 34th Gen. Assem. Sci. Symp. Int. Union Radio Sci. (URSI GASS)*, Aug. 2021, pp. 1–4.

[10] C. A. Balanis, *Antenna Theory: Analysis and Design*. Hoboken, NJ, USA: Wiley, 2016.

[11] H. C. Pocklington, "Electrical oscillations in wire," *Cambridge Phil. Soc. Proc.*, vol. 9, p. 324, Oct. 1897.

[12] E. Hallén, "Theoretical investigations into the transmitting and receiving qualities of antennae," in *Nova Acta Regiae Societatis Scientiarum Upsaliensis IV*, vol. 11, no. 4. Royal Society of Sciences of Upsala, 1938, pp. 3–44.

[13] J. E. Storer, "Impedance of thin-wire loop antennas," *Trans. Amer. Inst. Electr. Eng., I, Commun. Electron.*, vol. 75, no. 5, pp. 606–619, Nov. 1956.

[14] T. T. Wu, "Theory of the thin circular loop antenna," *J. Math. Phys.*, vol. 3, no. 6, pp. 1301–1304, Nov. 1962.

[15] H. Whiteside and R. King, "The loop antenna as a probe," *IEEE Trans. Antennas Propag.*, vol. AP-12, no. 3, pp. 291–297, May 1964.

[16] K. Iizuka, "The circular loop antenna multiloaded with positive and negative resistors," *IEEE Trans. Antennas Propag.*, vol. AP-13, no. 1, pp. 7–20, Jan. 1965.

[17] A. F. McKinley, "Theory of impedance loaded loop antennas and nanorings from RF to optical wavelengths," *IEEE Trans. Antennas Propag.*, vol. 65, no. 5, pp. 2276–2281, May 2017.

[18] P. L. Overfelt, "Near fields of the constant current thin circular loop antenna of arbitrary radius," *IEEE Trans. Antennas Propag.*, vol. 44, no. 2, pp. 166–171, Feb. 1996.

[19] D. H. Werner, "An exact formulation for the vector potential of a cylindrical antenna with uniformly distributed current and arbitrary radius," *IEEE Trans. Antennas Propag.*, vol. 41, no. 8, pp. 1009–1018, Jul. 1993.

[20] D. H. Werner, "An exact integration procedure for vector potentials of thin circular loop antennas," *IEEE Trans. Antennas Propag.*, vol. 44, no. 2, pp. 157–165, Feb. 1996.

[21] M. Kanda, "An electromagnetic near-field sensor for simultaneous electric and magnetic-field measurements," *IEEE Trans. Electromagn. Compat.*, vol. EMC-26, no. 3, pp. 102–110, Aug. 1984.

[22] M. Kanda and D. A. Hill, "A three-loop method for determining the radiation characteristics of an electrically small source," *IEEE Trans. Electromagn. Compat.*, vol. 34, no. 1, pp. 1–3, Feb. 1992.

[23] M. Rezaei, M. Baharian, and K. Mohammadpour-Aghdam, "An analysis of the magnetic field antenna," *IEEE Trans. Antennas Propag.*, vol. 69, no. 7, pp. 3654–3663, Jul. 2021.

[24] S. Khan, K. T. Wong, Y. Song, and W.-Y. Tam, "Electrically large circular loops in the estimation of an incident emitter's direction-of-arrival or polarization," *IEEE Trans. Antennas Propag.*, vol. 66, no. 6, pp. 3046–3055, Jun. 2018.

[25] D. R. Novotny, K. D. Masterson, and M. Kanda, "An optically linked three-loop antenna system for determining the radiation characteristics of an electrically small source," in *Proc. Int. Symp. Electromagn. Compat.*, 1993, pp. 300–305.

[26] S. Tofani, P. Ossola, G. d'Amore, L. Anglesio, M. Kanda, and D. R. Novotny, "A three-loop antenna system for performing near-field measurements of electric and magnetic fields from video display terminals," *IEEE Trans. Electromagn. Compat.*, vol. 38, no. 3, pp. 341–347, Aug. 1996.

[27] C. G. Hynes and R. G. Vaughan, "Electromagnetic loop sensor," in *Proc. Gen. Assem. Sci. Symp. (GASS) Int. Union Radio Sci.*, Rome, Italy, 2020, pp. 1–4.

[28] J. A. Stratton, *Electromagnetic Theory* (IEEE Press Series on Electromagnetic Wave Theory). Hoboken, NJ, USA: Wiley, 2007, p. 435.

[29] J. A. Stratton, *Electromagnetic Theory* (IEEE Press Series on Electromagnetic Wave Theory). Hoboken, NJ, USA: Wiley, 2007, p. 437.

[30] Dassault Systems. *CST Microwave Studio*. Accessed: Mar. 19, 2022. [Online]. Available: https://www.3ds.com/products-services/simulia/products/cst-studio-suite/

[31] G. N. Watson, *A Treatise on the Theory of Bessel Functions*, 2nd ed. Cambridge, U.K.: Cambridge Univ. Press, 1944.

[32] W.-X. Wang, "The exact kernel for cylindrical antenna," *IEEE Trans. Antennas Propag.*, vol. 39, no. 4, pp. 434–435, Apr. 1991.

[33] M. Abramowitz and I. A. Stegun, *Handbook of Mathematical Functions With Formulas, Graphs, and Mathematical Tables* (National Bureau of Standards Applied Mathematics Series), vol. 55. Washington, DC, USA: United States Department of Commerce, 1965.

[34] C. G. Hynes, "Reception of dipole sources using dual-loaded loop antennas," Ph.D. dissertation, School Eng. Sci., Simon Fraser Univ., Burnaby, BC, Canada, unpublished.

CHRISTOPHER G. HYNES (Student Member, IEEE) received the M.A.Sc. degree from The University of British Columbia, in 2007. He is currently pursuing the Ph.D. degree with the School of Engineering Science, Simon Fraser University. He was an Antenna/RF Engineer at companies, such as Nokia, Sierra Wireless, Fastback Networks, and Urthecast. He has experience with RF front-ends characterization and optimization, propagation link predictions, and antenna design. His successful designs include multiband cellular antennas, MIMO antennas, arrays, printed circuit board array feed networks (including substrate integrated waveguides), mmWave (60GHz) antennas, and antenna measurement systems. His current research interests include antennas, propagation, and bio-electromagnetics.

RODNEY G. VAUGHAN (Life Fellow, IEEE) is currently the Sierra Wireless Professor of communications with the School of Engineering Science, Simon Fraser University. His prior career in industrial research and development put a spotlight on the immense value of quality research, which ultimately drew him to academia. His research interests include information channels and the interplay between communications techniques, signal processing, and the physical aspects-the sensors, and the propagation and scattering of fields and waves. His current projects include theory, design, and evaluation methods for adaptive antenna systems and adaptive acoustic systems. He is a P.Eng.

• • •